PHYSICAL REVIEW E **84**, 011607 (2011)

Single crystal growth and anisotropic crystal-fluid interfacial free energy in soft colloidal systems

Van Duc Nguyen,[1] Zhibing Hu,[2] and Peter Schall[1,*]
[1]Van der Waals-Zeeman Institute, University of Amsterdam, Science Park 904, NL-1098 XH Amsterdam, The Netherlands
[2]Department of Physics, University of North Texas, Denton, Texas 76203, USA

(Received 6 February 2011; revised manuscript received 10 April 2011; published 15 July 2011)

We measure the anisotropy of the crystal-fluid interfacial free energy in soft colloidal systems. A temperature gradient is used to direct crystal nucleation and control the growth of large single crystals in order to achieve well-equilibrated crystal-fluid interfaces. Confocal microscopy is used to follow both the growth process and the equilibrium crystal-fluid interface at the particle scale: heterogeneous crystal nucleation, the advancing interface, and the stationary equilibrium interface. We use the measured growth velocity to determine the chemical potential difference between crystal and fluid phases. Well-equilibrated, large crystal-fluid interfaces are then used to determine the interfacial free energy and its anisotropy directly from thermally excited interface fluctuations. We find that while the measured average interfacial free energy is in good agreement with values found in simulations, the anisotropy is significantly larger than simulation values. Finally, we investigate the effect of impurities on the advancing interface. We determine the critical force needed to overcome impurity particles from the local interface curvature.

DOI: 10.1103/PhysRevE.84.011607 PACS number(s): 68.08.De, 81.10.Fq, 82.70.Dd

I. INTRODUCTION

The anisotropy of the crystal-melt interfacial free energy can be of critical importance to the morphological stability of crystal growth [1]. For most atomic crystals, this anisotropy is small, of the order of 2%, and is difficult to measure. The best results of the interfacial anisotropy come from simulations that take advantage of the change of thermally induced interface fluctuations to determine the anisotropy of the interfacial free energy [2–4]. While this technique provides a very sensitive measure of the anisotropy of the interfacial free energy, these fluctuations are too small to be measured in atomic systems. Recently, crystal-melt interfaces have been directly studied in colloidal suspensions by using confocal microscopy [5]. Because colloidal particles are several orders of magnitude larger than atoms, they can be studied in real time, and their positions in three dimensions can be tracked accurately by confocal microscopy. Nevertheless, in these previous experiments, the anisotropy of the interfacial free energy has not been resolved. Therefore, there still exists no direct experimental measurement of this anisotropy.

Here we resolve the anisotropy of the crystal-fluid interfacial free energy by using temperature-sensitive colloidal particles and a temperature field to grow large, equilibrated colloidal crystals. The temperature changes the effective size of the particles, thereby allowing precise control over crystal growth. We apply a temperature gradient to guide the nucleation of a few crystals, and slow cooling to direct the growth of these crystals. We use confocal microscopy to image the entire crystal growth process: heterogeneous crystal nucleation, the advancing crystal-fluid interface, and the stationary equilibrium crystal-fluid interface. We determine the amount of supersaturation that drives the growth of the crystals directly from the measured crystal growth velocity and the diffusion coefficient of particles in the liquid. We find that crystals grow perfectly at moderate supersaturations with a chemical potential difference $\Delta\mu \sim 0.4 k_{\mathrm{B}}T$ between the crystal and fluid. Flat crystal-fluid interfaces of large, equilibrated crystals are then investigated to determine the orientation dependence of the interfacial free energy. By analyzing height fluctuations of interfaces in different orientations, we determine an interfacial free energy per area of $\gamma = 0.70 k_{\mathrm{B}}T/d^2$, with an anisotropy of 1.6% for interfaces oriented perpendicular to the hexagonal close-packed plane. We use the measured value of the interfacial free energy to estimate the pressure and force acting on impurities at the interface. We determine a restoring force of 160 fN from the local interface curvature; this force is of the same order as forces determined for dislocation motion in colloidal crystals [6].

II. SYSTEM AND EXPERIMENTAL METHOD

We used poly-*N*-isopropylacrylamide (PNIPAM) colloidal particles which are cross-linked microgel spheres that are swollen in water at room temperature but shrink and undergo a reversible volume transition above the critical solution temperature [7]. The particle diameter changes reversibly from $d \sim 1.0\ \mu$m at room temperature to $d \sim 0.6\ \mu$m at 36.0 °C with a polydispersity of <3%. The particle density closely matches that of the solvent preventing settling of the particles for several weeks, while the close refractive-index match between the particles and the water makes the suspension transparent for observation with confocal microscopy. We prepared a dilute suspension of PNIPAM particles in a 5-mM NaCl solution that screened the particle charges, and subsequently concentrated the suspension by centrifugation at a high speed of 9000 rpm for 10 h. The close-packed suspension is then diluted slightly such that the resulting suspension is fully crystallized at room temperature, but the crystals melt entirely when the suspension is heated to 36 °C. We placed the suspension into $1 \times 2 \times 10\ \mathrm{mm}^3$ glass cells, which we sealed to avoid water evaporation. Two Peltier elements are used to create a temperature gradient across the cell. These Peltier elements, turned upside down with respect to each other, are connected to a thermal bath to independently set the average temperature

---

[*] pschall@science.uva.nl

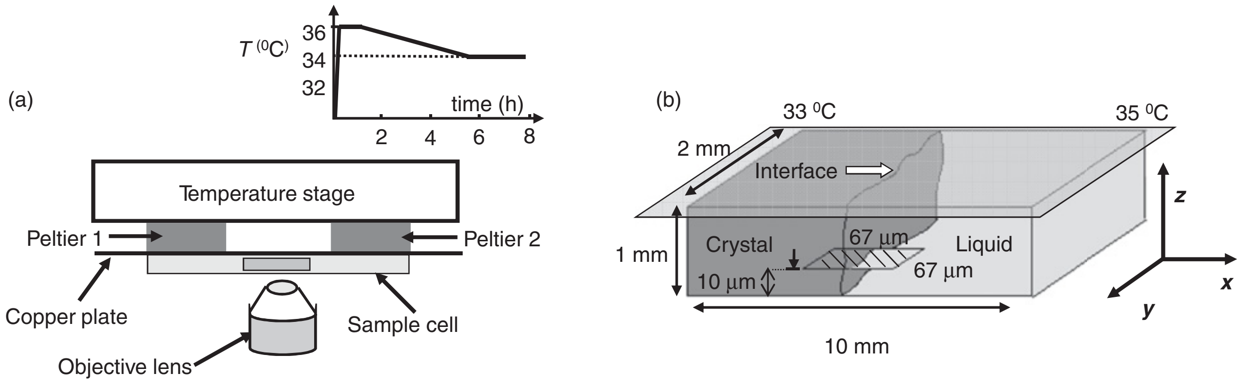

FIG. 1. Experimental setup and imaging. (a) Schematic of the temperature-gradient setup used to grow large colloidal crystals. The temperature stage controls the average temperature T, and the Peltier elements and copper plate create a linear temperature gradient around T across the sample. Inset: protocol of T as a function of time used for the single crystal growth. (b) Schematic showing the imaged 67 μm × 67 μm section (dashed) with respect to the sample cell. The dark gray color represents the crystals growing from left to right, while the light gray color represents the fluid. The x axis aligns with the temperature gradient direction.

and the temperature difference across the cell. A schematic of the setup is shown in Fig. 1(a). At room temperature, our sample was polycrystalline. We increased the average temperature to 36.0 °C, at which the crystals melted entirely, and we waited for 1 h to obtain a homogeneous colloidal melt. A temperature gradient of 2 °C/cm was then applied across the cell, and we lowered the average temperature of the sample slowly at a rate of 0.5 °C/h with a temperature stability of 0.02 °C to introduce nucleation and direct the growth of macroscopic single crystals. The temperature protocol is shown in the inset of Fig. 1(a). We used confocal microscopy to image individual particles in horizontal slices of 65 × 65 μm at the interface [see Fig. 1(b)]; these slices contain roughly 12 000 particles. The x axis aligns with the temperature-gradient direction. To avoid boundary effects, we focus on sections roughly 10 μm above the cover slip.

III. OBSERVATION OF NUCLEATION AND GROWTH

After 2 h of cooling, we observed that particles order in a few corners of the sample. Figure 2(a) shows that within the area indicated by the dotted line, the particles order on a lattice, while they are still disordered outside. We interpret these areas as heterogeneous crystal nuclei forming at the corners of the sample cell. Such heterogeneous nucleation reduces the interfacial area between the crystal and its melt, and is therefore energetically preferred over homogeneous nucleation in the bulk. We followed the development of these nuclei, and saw that they grew to large crystals while the effective particle volume fraction increased with decreasing temperature. Close inspection reveals that these crystals exhibit a random hexagonal close-packed (rhcp) structure. They consist of a random stacking of hexagonal close-packed (hcp) planes, similar to crystals formed in hard-sphere colloidal systems. The hcp planes align with the cover slip; their lateral orientation is random.

We focus on the early stage of crystal growth, and image the interface after $t_1 = 2.5$ h when the crystals have grown to 180 μm in length. Selected snapshots of the crystal-fluid interface during growth are shown in Figs. 2(b)–2(d). The interface advances in the positive x direction, while at the same time significant fluctuations of the interface occur. We determine the growth velocity by following the mean interface position as a function of time in Fig. 2(e). The data indicates linear growth with a constant velocity of $v = 0.1$ μm/s.

We follow the motion of the individual particles in the fluid and crystal to determine the diffusion coefficient. We acquire 200 images with a frame rate of 30 images/s and the positions of the individual particles in the horizontal sections are tracked with an accuracy of 0.03μm [8]. Particle trajectories are plotted in Fig. 3(a). While for particles in the fluid, these trajectories indicate diffusive motion; for particles in the crystal, they indicate confinement of the particles to their crystal lattice positions. For more clarity, we plot enlarged trajectories of a single particle in the crystal and fluid phase in the left- and right-hand insets of Fig. 3(a). We determine the mean square displacement $\langle r^2\rangle$ separately for particles in the crystal and fluid, and plot $\langle r^2\rangle$ as a function of time in Fig. 3(b). For crystal particles, the mean square displacement saturates at $\langle r^2\rangle_\infty = 0.0086$ μm^2 due to confinement by their neighbors, while for fluid particles $\langle r^2\rangle$ increases linearly with time, confirming that the particles exhibit diffusive motion. The asymptotic value of the crystal mean square displacement corresponds to twice the variance of the particles' displacement from their equilibrium position. We used this value to determine the three-dimensional Lindemann parameter of melting using [9] $L = \frac{1}{r_{\text{nn}}}\sqrt{\frac{3}{4}\langle r^2\rangle_\infty}$, where the crystal nearest-neighbor distance $r_{\text{nn}} = 0.7$ μm, assuming that particle fluctuations are isotropic. We find $L \sim 0.115$, in good agreement with values for close-packed crystals close to melting [10,11]. We also determined the diffusion coefficient D_{lq} of fluid particles from their mean square displacement using $\langle r^2\rangle \sim 4Dt$. A value of $D_{lq} = 0.052$ μm^2/s is obtained from the best linear fit [Fig. 3(b)]. The velocity of diffusion-limited growth can be estimated according to $v_{dl} = 4D_{lq}/d$ [12]. Using the measured diffusion coefficient, we obtain $v_{dl} = 0.3$ μm/s. This value is a factor of 3 larger than the observed growth velocity $v = 0.1$ μm/s indicating that the growth is not limited by diffusion. The difference between both values allows estimation of the amount of supersaturation

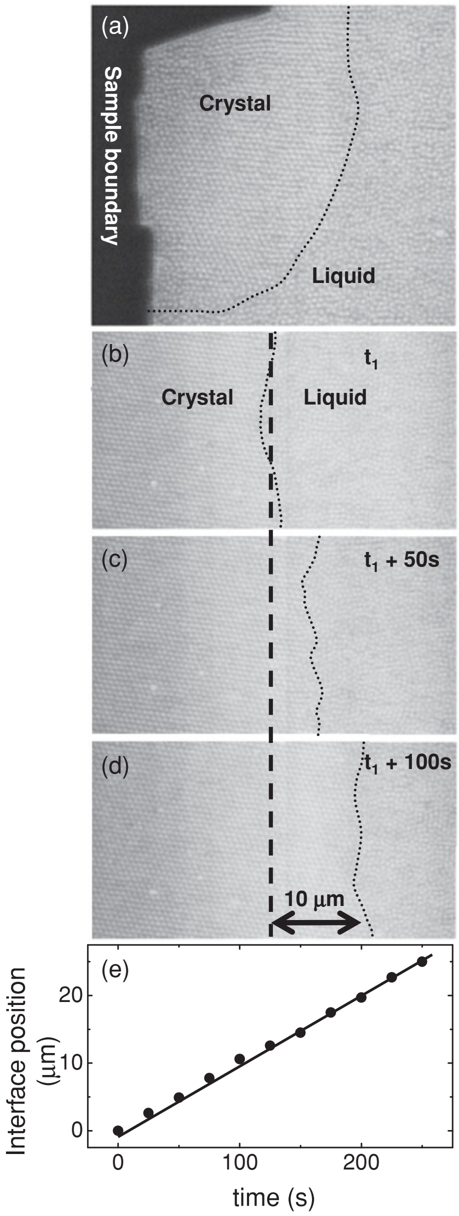

FIG. 2. Observation of crystal nucleation and growth. (a) Confocal microscope image of a crystal nucleus forming at the sample boundary. (b)–(d) Sequence of confocal microscope images taken during the early stage of crystal growth, starting after $t_1 = 2.5$ h of cooling. Dotted lines indicate the advancing interface, and the dashed line indicates the initial position of the interface at time t_1. (e) Mean interface position as a function of time, experimental measurements (dots), and best linear fit (solid line).

of the crystallizing suspension. We determine the chemical potential difference $\Delta\mu$ between fluid and crystal according to $\Delta\mu = -\ln(\frac{v_{dl}-v}{v_{dl}})k_B T$, assuming Wilson-Frenkel growth [13]. Using the experimentally measured values for v_{dl} and v, we find $\Delta\mu = 0.41 k_B T$, a small amount of supersaturation that indicates that the growth occurs close to the equilibrium freezing transition [12,14]. This value is in good agreement with simulation values between $0.2k_{\mathrm{B}}T$ and $0.5k_{\mathrm{B}}T$ for crystallizing soft spheres [15], and is of the same magnitude as hard-sphere simulation values predicted for $\phi \sim 0.52$ [16], well in the crystal-fluid coexistence regime.

IV. EQUILIBRIUM CRYSTAL-FLUID INTERFACE

The temperature-gradient technique allows us to prepare millimeter-size crystals with well-oriented flat interfaces; these are ideal to study intrinsic properties of the equilibrium crystal-fluid interface. After 4 h of cooling, when the crystals have reached several millimeters in length, we stopped the cooling and switched off the gradient to achieve equilibrium of macroscopic crystal and fluid phases. We focused on the stationary crystal-fluid interface and followed thermally induced fluctuations around its stable position. We acquired 200 images, and followed the fluctuations of the one-dimensional trace of the interface in the imaged section. A 67 μm × 67 μm confocal microscope image is shown in Fig. 4. To pinpoint the interface position $x = f(y)$ (dotted line), we distinguish crystal and fluid particles from their nearest-neighbor environment. For each particle, we find the nearest neighbors as those separated by a distance less than the first minimum of the pair correlation function, and we compare the nearest-neighbor vectors $\boldsymbol{d_i}$ with those of the reference crystal lattice vectors $\boldsymbol{D_i}$ [see top left inset of Fig. 4(a)]. Deviations from the reference vectors are determined using the order parameter [2] $\delta^2 = \frac{1}{6}\sum_i (d_i - D_i)^2$, the mean square difference between the actual and the reference nearest-neighbor vectors. To find the interface position $x = f(y)$, we define a grid in the x-y plane with a mesh size $\Delta x = \Delta y = d = 0.7\mu$m and calculate the order parameter for each grid point as the average order parameter of particles with centers within $2.5d$ in the x direction and $1.5d$ in the y direction from the center of the grid point [see bottom left of Fig. 4(a)]. We plot the average order parameter as a function of x in the upper right inset of Fig. 4(a). This order parameter increases from $\delta^2 \sim 0.02\ d^2$ in the crystal to $\delta^2 \sim 0.12\ d^2$ in the fluid, indicating the loss of crystalline order. We define the interface position x_{I} from the requirement $\delta^2(x_{\mathrm{I}}) = 0.07d^2$ (dashed lines in the inset) which is halfway between the values of the bulk crystal and fluid phases [3], and plot a reconstruction of the crystal-fluid interface in Fig. 4(b). Gray dots show particles with order parameter values $\delta^2 < 0.07d^2$, while open circles indicate particles with $\delta^2 > 0.07d^2$. The black line is obtained by connecting all points with order parameter $\delta^2 \sim 0.07d^2$, and indicates the trace of the crystal-fluid interface in the plotted section. A few traces of reconstructed interfaces are shown in Fig. 4(c); these show the thermally induced fluctuations of the interface around a stable position. Gray lines indicate instantaneous interface positions, and the solid black line indicates the time-averaged interface. In thermal equilibrium, interface waves with wave vector q are excited with mean square amplitude $\langle |A_q|^2\rangle = k_{\mathrm{B}}T/[bl(\gamma+\gamma'')q^2]$, where $(\gamma+\gamma'')$ is the interface stiffness, and b and l are the thickness and width of the imaged section [2,17]. We determine the average spectrum A_q of interfacial fluctuations by Fourier transformation of the individual interface profiles. This analysis is then repeated for several different interface orientations to determine the orientation-dependent interface stiffness. Average interface spectra $\langle |A_q|^2\rangle$ as a function of q^2 for three selected interface orientations are shown in Fig. 5(a).

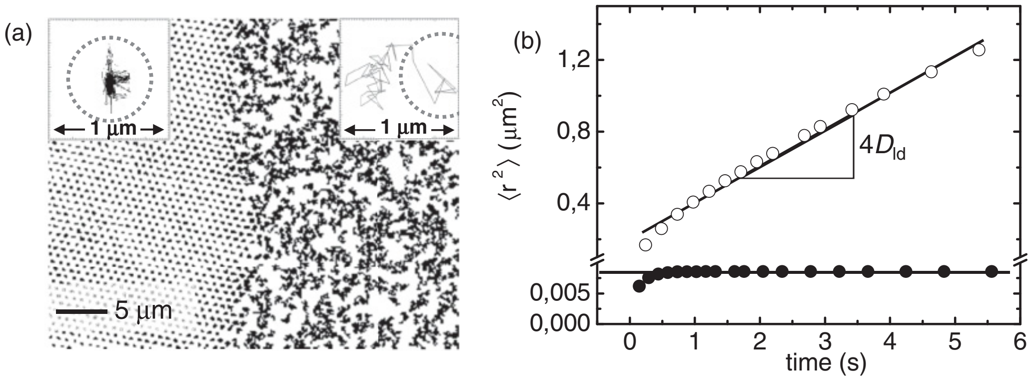

FIG. 3. Particle trajectories and mean square displacement. (a) Trajectories of particles in the crystal (left) and fluid (right). Inset: enlargement of a single particle trajectory for a particle in the crystal (top left) and fluid (top right). (b) Mean square displacement as function of time for particles in the crystal (filled dots) and fluid (open dots). The mean square displacement of crystal particles saturates at a value of 0.0086 μm^2 (solid line, bottom), while that of fluid particles increases linearly with time (solid line, center) indicating diffusion. The slope equals four times the diffusion coefficient.

The data confirm the decay $A_q^2 \propto q^{-2}$ for all orientations. We notice a systematic shift of the data in the double-logarithmic representation; this shift indicates the change of the interface stiffness with orientation. To determine the corresponding stiffness values, we plot $(\langle |A_q|^2 \rangle lb)^{-1}$ as a function of q^2 in a linear representation in Fig. 5(b). A clear distinction of three slopes indicates the clear difference of interfacial stiffness for the three orientations. Values of the interface stiffness are obtained from the best linear fit to the data [solid lines in Fig. 5(b). We analyzed interfacial spectra of many more interface orientations and list the corresponding stiffness values and error margins, obtained from a linear regression analysis of the data in Table I. Here, the error bars indicate one standard deviation of uncertainty. We note that an additional source of systematic error can come from the choice of the threshold value δ. Thresholds of $\delta^2 = 0.05d^2$ and $0.09d^2$ instead of the chosen value $0.07d^2$ lower the stiffness values by $\sim$5%.

These stiffness values vary systematically with crystal orientation. For the orientation-dependent stiffness follows $\gamma + \gamma'' = \gamma_0[1 + \varepsilon \cos(\alpha)]$, reflecting the average sixfold symmetry of the rhcp crystal. Here, γ_0 and ε are the average interfacial free energy per area and its anisotropy, respectively. For the orientation-dependent stiffness follows $\gamma + \gamma'' = \gamma_0[1 - 35\varepsilon \cos(6\alpha)]$. Our measured values are in excellent agreement with this prediction as shown by plotting the interface stiffness as a function of $\cos(6\alpha)$ in Fig. 5(c). We determine values of $\gamma_0 = (0.70 \pm 0.10)k_{\rm B}T/d^2$ and $\varepsilon = (0.016 \pm 0.004)$ from the best linear fit to the data (solid line). The value of γ_0 can be compared with the orientational average of interfacial free energies obtained in simulations for interfaces perpendicular to the hcp plane. For soft-sphere crystal-fluid interfaces, these simulations find values between $0.55k_{\rm B}T/d^2$ and $0.8k_{\rm B}T/d^2$ depending on the particle softness [18], in good agreement with our measurement. The magnitude of the anisotropy, however, is much larger than simulation values of anisotropies within the hexagonal close-packed plane. We estimate the anisotropy within the hcp plane for simulated fcc crystal-liquid interfaces by using the full cubic harmonic expansion of the interfacial free energy determined in the simulations [3]. Using the orthogonal directions $[\bar{1}10]$ and $[11\bar{2}]$ along the hcp plane, we determine that these simulations predict an anisotropy of (0.25 ± 0.21)% within the hcp plane for hard-sphere fcc crystals [3]. We also compare our value to simulation values of magnesium [4], which has hexagonal crystal structure. These simulations find an anisotropy of (0.18 ± 0.08)% for interfaces perpendicular to the hcp plane [4]. Our measured value of (1.6 ± 0.4)% is significantly larger than both these predictions.

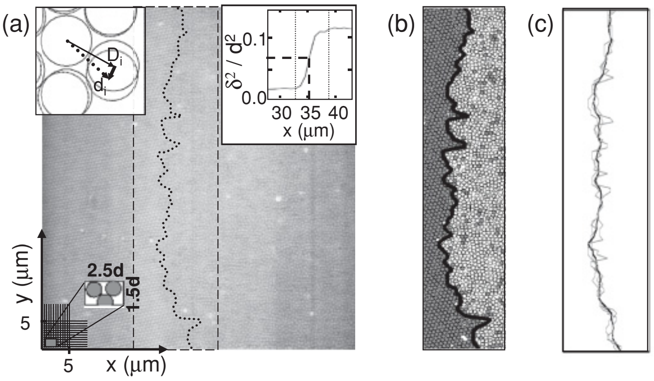

FIG. 4. Equilibrium interface and interface fluctuations. (a) Confocal microscope image of the stationary crystal-fluid interface. The upper left inset illustrates the determination of the order parameter from the nearest-neighbor vectors $\boldsymbol{d}_{\rm i}$, and the reference vectors $\boldsymbol{D}_{\rm i}$. The lower left inset illustrates the coarse graining procedure of the order parameter. Upper right inset: Order parameter as a function of x across the interface. The dotted lines, at $x = 33$ μm and $x = 38$ μm, indicate the interfacial width $w \sim 6d$, while the dashed lines indicate the interface position. (b) Reconstruction of the crystal-fluid equilibrium and interface. Gray dots represent particles with a crystalline environment, while circles represent particles with a fluidlike environment. The black solid line indicates the interface. (c) Snapshots of the interface (gray) demonstrating fluctuations around the average position (black).

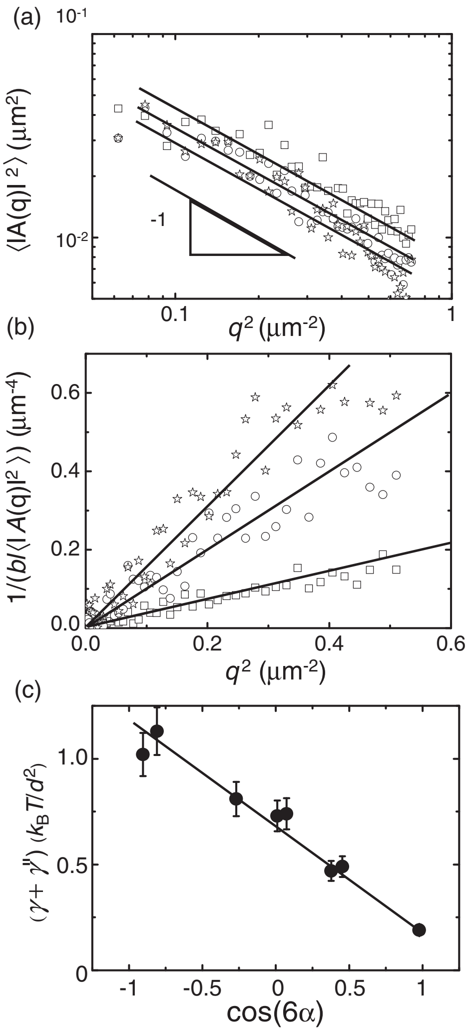

FIG. 5. Spectrum of interfacial fluctuations. (a) Log-log plot of the fluctuation spectra for the crystal orientations $\alpha = 2^\circ$ (squares), 10.5° (circles), and 14.9° (stars). The solid lines indicate a slope of –1. (b) $1/bl\langle |A(q)|^2\rangle$ vs q^2 for the three crystal orientations. The solid lines indicate best linear fits to the data. (c) Interface stiffness as a function of $\cos(6\alpha)$. The slope of the best linear fit (solid line) equals 35 times the anisotropy.

V. CRYSTAL GROWTH STABILITY

We also investigated the role of the interfacial free energy in stabilizing the crystal growth. This was achieved by adding "impurity particles" that act as obstacles and pin the advancing interface. We added impurity particles of two different sizes, with radii $R_1 \sim 2d$ and $R_2 \sim 3d$, and followed the interface with time starting from the moment where the interface reaches the edge of the impurities [Fig. 6(a)]. We observe that both impurities pin the interface; however, while the small impurity is easily overcome by the interface, the larger impurity holds the advancing interface back and causes it to bow strongly [Figs. 6(b) and 6(c)]. The interface curvature leads to a local force $F = PA_{\text{eff}}$ that tries to drive the interface across the obstacle. Here, A_{eff} is the effective contact area between the interface and the obstacle, and P can be estimated from the Laplace pressure $P_{\text{LP}} = 2\gamma/R_{\text{c}}$, with R_{c} the radius of curvature of the pinned interface. The interface overcomes the impurity when the driving force F becomes larger than F_{obst}, the critical force required to surmount the obstacle. This critical force is $F_{\text{obst}} \sim 2\gamma A_{\text{eff}}/R_{\text{c}}$, where we take $R_{\text{c}} \sim R_2$ and the contact area $A_{\text{eff}} = (4\pi R_2)^2/2$. Using $\gamma = 0.71 k_B T/d^2$ for the crystal orientation $\alpha = 14.9^\circ$, we obtain $F_{\text{obst}} = 1.6 \times 10^{-13}$ N. This force is of the same order as that measured for dislocation motion through a dense colloidal crystal [6]. When $F > F_{\text{obst}}$, the interface overcomes the impurity, and it quickly retracts and flattens, thereby minimizing its energy cost [Fig. 6(d)].

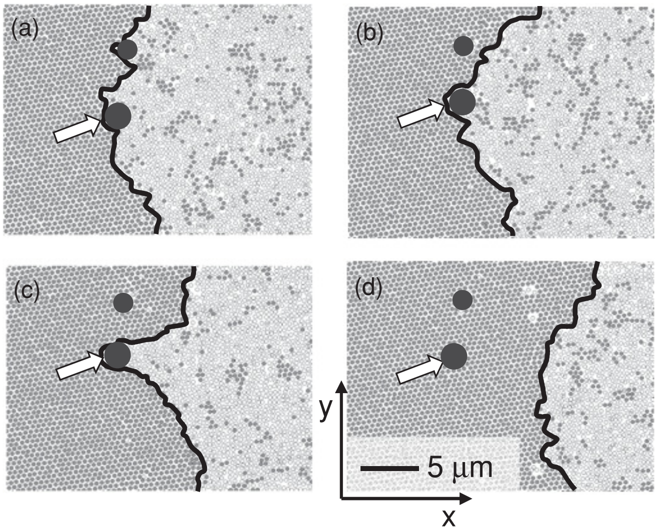

FIG. 6. Crystal growth across impurities. (a)–(d) Sequence of reconstructed images showing the advancing solid-fluid interface surmounting impurity particles (dark gray spots): Interface touching the impurities (a), surmounting the small impurity (b), pinned by the large impurity (c), and final straightening of the interface after successful transgression (d).

VI. CONCLUSION

The temperature sensitivity of PNIPAM hydrogel particles allows excellent control to guide macroscopic crystal growth. We have shown that in analogy to atomic crystal growth, large macroscopic PNIPAM colloidal crystals grow in a temperature gradient when the suspension is cooled slowly so that only a few crystal nuclei form initially. We followed the growth directly and determined a chemical potential difference of

TABLE I. Orientation-dependent interface stiffness. Measured interface stiffness $(\gamma+\gamma q'')$ for several crystal orientations α. α denotes the angle between the normal of the crystal-fluid interface, and a nearest-neighbor vector in the hcp plane.

α (degrees)	$(\gamma+\gamma q'')$ $(k_B T/d^2)$
2.0	0.19 ± 0.02
10.5	0.49 ± 0.05
14.3	0.74 ± 0.08
14.9	0.73 ± 0.08
24.0	1.13 ± 0.12
34.2	1.02 ± 0.01
42.4	0.81 ± 0.09
48.7	0.47 ± 0.05

$\Delta\mu = 0.41k_BT$ between crystal and fluid phases indicating that the growth occurred close to equilibrium with only moderate undercooling.

The well-equilibrated interfaces of large crystals allowed us to experimentally resolve the anisotropy of the solid-fluid interfacial free energy. From the fluctuations of interfaces with various orientations, we determined an interfacial free energy of $\gamma = 0.70k_\mathrm{B}T/d^2$ with an anisotropy of 1.6% within the hexagonal close-packed plane. The average value is in good agreement with simulation values, contrary to earlier experimental studies on hard-sphere colloidal crystals grown under sedimentation in gravity, indicating that gravity might have affected these earlier measurements. The value of the anisotropy $\varepsilon = 1.6\%$ is significantly larger than simulation values found for the interfacial anisotropy within the hexagonal close-packed plane.

ACKNOWLEDGMENTS

This work was supported by the Innovational Research Incentives Scheme (VIDI grant) of the Netherlands Organization for Scientific Research (NWO).

[1] J. Lipton, M. E. Glicksman, and W. Kurz, Mater. Sci. Eng. **65**, 57 (1989); W. J. Boettinger, S. R. Coriell, A. L. Greer, A. Karma, W. Kurz, M. Rappaz, and R. Trivedi, Acta Mater. **48**, 43 (2000); J. J. Hoyt, M. Asta, and A. Karma, Mater. Sci. Eng., R **41**, 121 (2003).

[2] J. J. Hoyt, M. Asta, and A. Karma, Phys. Rev. Lett. **86**, 5530 (2001).

[3] R. L. Davidchack, J. R. Morris, and B. B. Laird, J. Chem. Phys. **125**, 094710 (2006).

[4] D. Y. Sun, M. I. Mendelev, C. A. Becker, K. Kudin, T. Haxhimali, M. Asta, J. J. Hoyt, A. Karma, and D. J. Srolovitz, Phys. Rev. B **73**, 024116 (2006).

[5] J. Hernandez-Guzman and E. R. Weeks, Proc. Natl. Acad. Sci. USA **106**, 15198 (2009); I. B. Ramsteiner, D. A. Weitz, and F. Spaepen, Phys. Rev. E **82**, 041603 (2010); U. Gasser *et al.*, Science **292**, 258 (2001).

[6] P. Schall *et al.*, Science **305**, 1944 (2004).

[7] R. H. Pelton, Adv. Colloid Interface Sci. **85**, 1 (2000); H. Senff and W. Richtering, J. Chem. Phys. **111**, 1705 (1999); Z. B. Hu, X. H. Lu, and J. Gao, Adv. Mater. **13**, 1708 (2001).

[8] E. R. Weeks *et al.*, Science **287**, 627 (2000).

[9] A. M. Alsayed *et al.*, Science **309**, 1207 (2005).

[10] F. A. Lindemann, Z. Phys. **11**, 609 (1910); R. W. Cahn, Nature **413**, 582 (2001).

[11] D. A. Young and B. J. Alder, J. Chem. Phys. **60**, 1254 (1974); R. Ohnesorge, H. Löwen, and Wagner, Europhys. Lett. **22**, 245 (1993).

[12] D. J. W. Aastuen, N. A. Clark, L. K. Cotter, and B. J. Ackerson, Phys. Rev. Lett. **57**, 1733 (1986).

[13] H. A. Wilson, Philos. Mag. **50**, 238 (1900); J. Frenkel, Phys. Z. Sowjetunion **1**, 498 (1932).

[14] M. Würth, J. Schwarz, F. Culis, P. Leiderer, and T. Palberg, Phys. Rev. E **52**, 6415 (1995); T. Palberg, J. Phys.: Condens. Matter **11**, R323 (1999)

[15] S. Auer, W. C. K. Poon, and D. Frenkel, Phys. Rev. E **67**, 020401 (2003).

[16] S. Auer and D. Frenkel, J. Chem. Phys. **120**, 3015 (2004).

[17] M. P. A. Fisher, D. S. Fisher, and J. D. Weeks, Phys. Rev. Lett. **48**, 368 (1982).

[18] R. L. Davidchack and B. B. Laird, Phys. Rev. Lett. **85**, 4751 (2000); **94**, 086102 (2005).